Aryltriazene photopolymer thin films as sacrificial release layers for laser-assisted forward transfer systems

Study of photoablative decomposition and transfer behavior

Originally published in:
Applied Physics A 92(4), https://doi.org/10.1007/s00339-008-4565-4

Appl Phys A (2008) 92: 781–789
DOI 10.1007/s00339-008-4565-4

Applied Physics A
Materials Science & Processing

Aryltriazene photopolymer thin films as sacrificial release layers for laser-assisted forward transfer systems: study of photoablative decomposition and transfer behavior

Matthias Nagel · Romain Fardel · Pascal Feurer · Mark Häberli · Frank A. Nüesch · Thomas Lippert · Alexander Wokaun

Received: 12 October 2007 / Accepted: 4 March 2008 / Published online: 22 May 2008

Abstract Thin films of a tailor-made photodecomposible aryltriazene polymer were applied in a modified laser-induced forward transfer (LIFT) process as sacrificial release layers. The photopolymer film acts as an intermediate energy-absorbing dynamic release layer (DRL) that decomposes efficiently into small volatile fragments upon UV laser irradiation. A fast-expanding pressure jet is generated which is used to propel an overlying transfer material from the source target onto a receiver. This DRL-assisted laser direct-write process allows the precise deposition of intact material pixels with micrometer resolution and by single laser pulses. Triazene-based photopolymer DRL donor systems were studied to derive optimum conditions for film thickness and laser fluences necessary for a defined transfer process at the emission wavelength of a XeCl excimer laser (308 nm). Photoablation, surface detachment, delamination and transfer behavior of aryltriazene polymer films with a thickness from 25 nm to ∼400 nm were investigated in order to improve the process control parameters for the fabrication of functional thin-film devices of microdeposited heat- and UV-sensitive materials.

PACS 52.38.Mf · 42.62.-b · 81.15.Fg · 85.40.Hp

M. Nagel (✉) · R. Fardel · P. Feurer · M. Häberli · F.A. Nüesch
Empa, Swiss Federal Laboratories for Materials Testing and Research, Laboratory for Functional Polymers, Überlandstrasse 129, 8600 Dübendorf, Switzerland
e-mail: matthias.nagel@empa.ch

R. Fardel · T. Lippert · A. Wokaun
Paul Scherrer Institut, General Energy Research Department, 5232 Villigen PSI, Switzerland

1 Introduction

Laser-based direct-writing and printing operations are finding increasingly applications for precise surface micromodification techniques by either controlled ablation processes or the tailored deposition of complex materials, as outlined in Fig. 1. Several methods have been developed for the targeted deposition of a broad range of various materials applying lasers [1]. Among them, pulsed laser deposition (PLD) can be used grow films of inorganic [2, 3] or organic materials [4–7] on a substrate. Matrix-assisted pulsed laser evaporation (MAPLE) is used for the gentle deposition of small molecules trapped in a frozen solvent matrix [7, 8]. A further versatile direct-writing method for the accurate microdeposition of a variety of different materials is based on laser-induced forward transfer (LIFT) techniques [9–11]. In conventional LIFT setups, a transparent carrier is coated with a layer of the material to be transferred and placed closely to a receiver substrate. Irradiation of a defined spot of the source target by a focused laser pulse coming in through the carrier triggers the mass transfer towards the receiver, as depicted in Fig. 1b. By absorption of the laser photons, the transfer material itself is locally heated and a forward-ejection is caused by generating an evaporative pressure jet within the transfer layer. With this basic LIFT processing, patterns of mainly robust and heat-resisting materials that tolerate such phase transformations could be directly transferred onto various types of receiver substrates. The high intrinsic thermal stress generated within the irradiated layer during the mass transfer step can induce decomposition or disintegration of more complex materials to be deposited. Attempts to apply original LIFT methods for the controlled pixel deposition of sensitive materials, such as biomaterials, viable cells or also semiconducting polymers proved to be limited by their

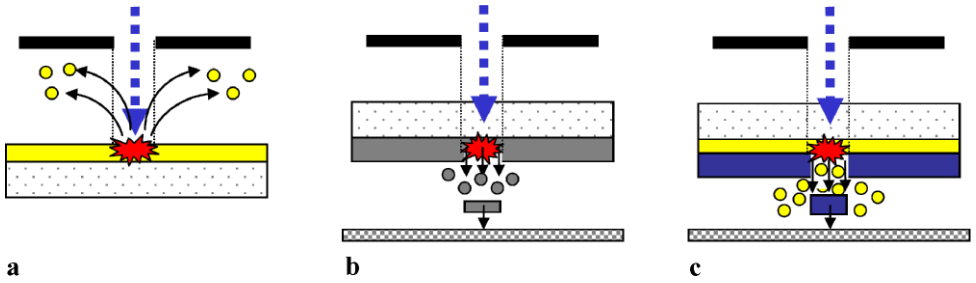

Fig. 1 Basic experimental setups for conventional laser ablation (**a**), and laser-induced forward transfer (LIFT) processes (**b**). For the LIFT setup the transfer material has to be coated onto a transparent carrier substrate to enable a forward ablation by irradiation from the backside through the carrier. In traditional LIFT setups (**b**) the material to be transferred is exposed to the incident laser, and is required to act as its own propellant whereas in setup (**c**) an intermediate sacrificial dynamic release layer (DRL) absorbs the laser energy. Laser-induced decomposition of the DRL provides the thrust for propelling the top layer onto the receiving substrate

proneness to heat damage or direct laser exposition [1, 12–15]. In order to prevent the transfer layer from direct laser exposition, intermediate laser absorbing layers were introduced to assist the forward transfer process when applied to materials that cannot be directly evaporated or melted [16]. As outlined in Fig. 1c, such dynamic release layer (DRL) systems serve as energy-absorbing sacrificial layers that decompose upon laser irradiation and provide the thrust for propelling the top layer onto the receiver [17]. The use of thin intermediate films of metals (e.g., Ag, Au, Ti) or metal oxides (e.g., TiO_2) has been reported as absorbing layers for UV laser-based forward transfer applications of biomolecules [18–21] and cells [12, 22], in the literature referred to as absorbing film assisted (AFA) LIFT [23–25] and Biological Laser Printing (BioLP^{TM}) [12, 26]. Various polymeric composite materials (usually a binder matrix doped with dispersed absorber dyes) have been applied as DRL systems mostly in conjunction with powerful IR lasers, e.g., for high-resolution full-color printing [27–29] and the microdeposition of electronic materials [30–34]. However, such intermediate absorbing light-to-heat conversion layers could not completely reduce the intrinsically high thermal load on sensitive transfer materials during the thermo-propulsive transfer process [31–34]. For all these DRL-based LIFT systems, it is important that the decomposition products of such additional intermediate sacrificial absorbing layers will not contaminate the transferred layer, as, e.g., observed for metal absorbing film-assisted (AFA) LIFT methods [25].

In order to avoid such drawbacks from either substrate contaminations or thermal transfer defects [34], we have recently developed and tested a modified concept of the LIFT process based on thin sacrificial absorbing layers made of designed UV-sensitive aryltriazene photopolymers [35–37]. Aryl-dialkyltriazene polymer films show a high absorption in the range of ~250–350 nm and can be efficiently decomposed and ablated when irradiated with UV lasers [35]. From the chemical structure formula shown in Fig. 2 it can be seen that two photocleavable aryltriazene (Ar–N=N–N–)

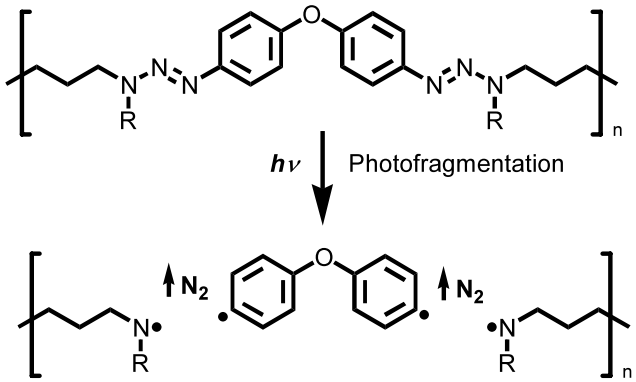

Fig. 2 Structure formula of the studied photopolymer TP-6-Me (R = CH_3). Two photodecomposible aryltriazene chromophores per repeating unit are covalently incorporated into the polymer main chain, joined by an alkyl bridge. Upon UV irradiation the triazene moiety is homolytically cleaved, leading to a fragmentation of the polymer backbone and evolution of elemental nitrogen

chromophores per repeating unit are covalently incorporated into the polymer main chain. Exposure to UV irradiation causes a photolytic cleavage of the triazene chromophores which leads to an irreversible evolution of elemental nitrogen and simultaneously to the fragmentation of the polymer into small molecules. Therefore, films of these photosensitive polymers proved to be excellently suitable for laser ablation applications since they can be cleanly ablated without carbonization or redeposition of debris already at fluences far below 100 mJ/cm^2 [35, 36]. The laser-triggered photofragmentation process results in an abrupt volume expansion. This effect can be utilized for LIFT applications where the generated pressure jet then propels the overlaying film of pure transfer material towards the receiver surface, as outlined in Fig. 1c.

Due to its favorable ablation characteristics [35] aryltriazene photopolymer TP-6-Me became an important reference compound for mechanistic studies on laser ablation of polymers within the last decade. Applied as a thin

dynamic release layer (DRL), the promising potential of the high-quality photopolymer films was demonstrated recently: Assisted by a ∼100 nm thick sacrificial DRL of our reference aryltriazene photopolymer TP-6-Me, viable mammalian neuroblast cells were transferred and gently deposited on a bioreceiver substrate [38]. In a similar manner, laterally well-resolved arrays of multispectral nanocrystal quantum dots (NCQD) were successfully transferred [39], as well as pixel patterns of electroluminescent polymers for the fabrication of light-emitting electronic devices (OLEDs) [40]. In order to adapt novel fields of transfer applications, we are studying the influence of the various process parameters and effects of individual material properties on the performance of the DRL-based LIFT systems [41, 42]. The triazene-based sacrificial polymer release layer systems have to be optimized with regard to film forming, surface compatibility, interface adhesion, optimum film thickness of the DRL in relation to the thickness of a specific transfer material layer at a given laser wavelength and fluence. Here we focus at first on thin films of our reference photopolymer TP-6-Me and report on the characterization of its photoablative decomposition, the surface perforation and delamination behavior in basic LIFT experiments as well as the resulting surface morphology after laser treatment in forward transfer experiments.

2 Experimental

Aryltriazene homopolymer TP-6-Me was synthesized according to our improved general protocol published earlier [37]. Smooth and crack-free, homogeneously transparent films with an easily controllable thickness between ∼20 nm and up to more than 500 nm were prepared by spin-coating polymer solutions (in a 1:1 wt/wt mixture of cyclohexanone and chlorobenzene) onto quartz substrates (Suprasil 2 fused silica) in a laminar flow hood, as described in [37]. Film thicknesses and surface roughness measurements were performed on a profilometer (Ambios XP-1, tip radius 2.5 µm), with a stylus force of 0.05 mg. Micrographs were taken by an optical microscope (Zeiss Axioplan) coupled with a digital camera system (Leica DC500). Ablation experiments were performed with a XeCl excimer laser (Compex, Lambda Physik, $\lambda = 308$ nm, $\tau = 30$ ns), and the fluence was controlled by an attenuator plate. A homogeneous part of the beam was imaged by a quartz lens onto the polymer film surface (magnification 0.25), and the geometry of the ablated spots defined by a rectangular mask (aperture 2 mm), yielding a spot size of 500 µm × 500 µm. Pulse energies at each fluence were measured by a pyroelectric energy meter (Molectron J4-09 or Gentec QE 50), and averaged over 100 pulses. Variation of the single pulse energies were typically in the range of ±10%.

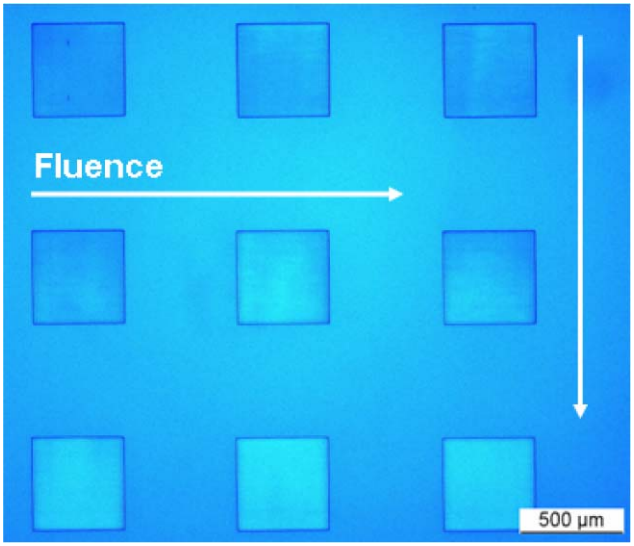

Fig. 3 Microscope image of a part of a 420 nm thick film of TP-6-Me with a typical ablation matrix created according to the classical setup in Fig. 1a. Each spot was ablated by a single pulse at 308 nm with increasing laser fluences between ∼20 mJ/cm^2 and ∼180 mJ/cm^2

For ablation experiments, films coated on quartz substrates were mounted on a translation stage perpendicular to the laser beam and irradiated with the film side oriented towards the incident laser. For transfer experiments, the donor and the receiver substrate were placed in close contact (<1 µm), and the beam was focused onto the backside of the donor substrate. A matrix of rectangular ablation spots was created on each film sample supported by a computer-controlled system that allowed variation of the pulse energy.

Linear decadic absorption coefficient a of polymer films at the laser emission wavelength was determined by dividing the absorbance at 308 nm (measured with a Cary-50 spectrophotometer) by the film thickness (measured by profilometry) and was found to be ≈93 000 cm^{-1} for the polymer TP-6-Me. By conversion from the conventional log scale base for absorption measurements to the natural logarithm (ln) the corresponding absorption coefficient α is ∼215 000 cm^{-1}.

3 Results and discussions

3.1 Study of ablation characteristics

In order to derive basic process parameters for the application as sacrificial absorbing layers in advanced LIFT systems, the photoablation behavior of thin films of the well-characterized aryltriazene photopolymer TP-6-Me [37] as our current standard basic compound was studied. Spots with a size of about 500 µm × 500 µm were ablated in a 420 nm thick polymer film using single pulses of a XeCl

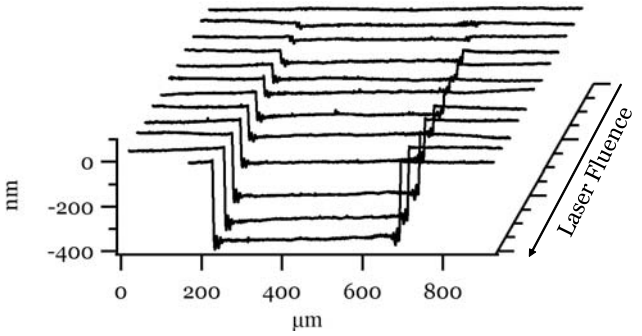

Fig. 4 Compilation of profilometry traces of ablated spots created by a single pulse in a 420 nm thick film of TP-6-Me at 12 increasing laser fluences of 20, 24, 28, 32, 36, 40, 49, 61, 87, 125, 154, 181 mJ/cm^2, corresponding to traces 1 to 12, respectively. The onset of the polymer ablation can be clearly recognized in the second trace at 24 mJ/cm^2

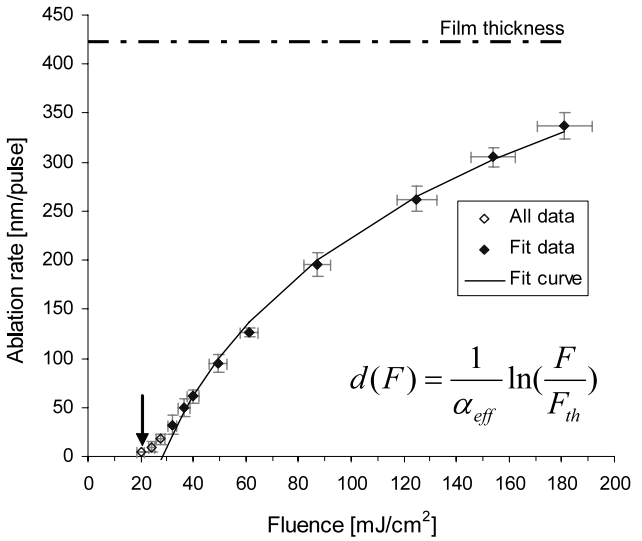

Fig. 5 Correlation between ablation depths and applied laser fluence per pulse for spots ablated by a single pulse derived from profilometry analyses shown in Fig. 4. The horizontal error bars indicate the pulse-to-pulse average variation of the laser fluence, whereas the vertical bars reflect the deviation range of the crater depths. The fluence threshold for ablation is below 24 mJ/cm^2 (indicated by the *arrow*). The curve represents the fit with the shown empirical formula for the ablation rate (see text) at laser fluences above ~32 mJ/cm^2

excimer laser. In Fig. 3, a microscopy image of a part of a typical ablation matrix is shown, demonstrating the homogeneous morphology of the layer surface as well as the high quality of the ablated structures with sharp and clear-cut rims. No carbonization or redeposition of ablated particle fragments (debris formation) was found, proving the high performance of the ablation process of such photopolymers [35, 36]. A compilation of profilometry traces of the resulting crater depths as well as the surface morphology inside the pits is shown in Fig. 4 for laser fluences between 20 mJ/cm^2 and 180 mJ/cm^2. The threshold fluence (F_{th}) of the ablation onset was found to be below 24 mJ/cm^2, and the ablated spots exhibit regular pot-type geometries without any formation of protruding burrs along the upper edges of the pits. The surface morphology of the crater bottoms appears homogeneously smooth and flat. The determined ablation depths d per pulse are plotted versus the corresponding laser fluences F in the graph shown in Fig. 5. The values for the ablation depths $d(F)$ at laser fluences between ~30 mJ/cm^2 and 180 mJ/cm^2, give the characteristic ablation curve which can be fitted well with the phenomenological equation

$$d(F) = \alpha_{\text{eff}}^{-1} \ln(F/F_{\text{th}}), \quad (1)$$

where d is the ablation rate, α_{eff} the effective absorption coefficient, F the fluence and F_{th} the threshold fluence [35, 36]. From the fit curve analysis of our data, we derive as the extrapolated ablation threshold fluence $F_{\text{th}} \approx 28$ mJ/cm^2 and as the formal value for the effective absorption coefficient for ablation $\alpha_{\text{eff}} \approx 56\,000$ cm^{-1}. This value for α_{eff} is about 25% of the corresponding ln-based absorption coefficient α of ~215 000 cm^{-1} which was determined by photometry for static UV irradiation with light intensities far below the ablation regime. The lower value of α_{eff} reflects the observations that the photodecomposition process of absorbing triazene chromophores starts already within the 30 ns time scale of the pulsed laser irradiation and causes therefore a nominally larger dynamic penetration depth of the incident pulse [35, 43].

3.2 Characterization of "forward ablation"

For the application of the photopolymer films as sacrificial absorbing release layers the experimental setup of the laser target has to be turned by 180°, according to Fig. 1b. Now, the photon interaction with the polymer film starts from the reversed side at the substrate-film interface. The laser-induced decomposition of films of TP-6-Me with different thicknesses were characterized under these inversed conditions, first without the presence of a receiver, as depicted by sketch series A and B in Fig. 6. The incident laser pulse causes an abrupt local photodecomposition within the polymer film volume, and one has to take into account the exponential decay of the absorbed light intensity at increasing propagation length. At first, the gaseous photofragmentation products are trapped in the spot cavity volume between the carrier substrate and the remaining overlying film, as depicted in sketch d in Fig. 6. As a consequence, the abrupt volume expansion within the hollow spot generates a pressure jump. It depends now on the thickness of the film and the applied fluence whether the laser-triggered volume expansion is sufficient enough to perforate and ablate the whole film volume or to lift-off and forward-eject a remaining top layer (cf. sketches c and g, respectively, in Fig. 6). This requires that the impact of the released pressure thrust

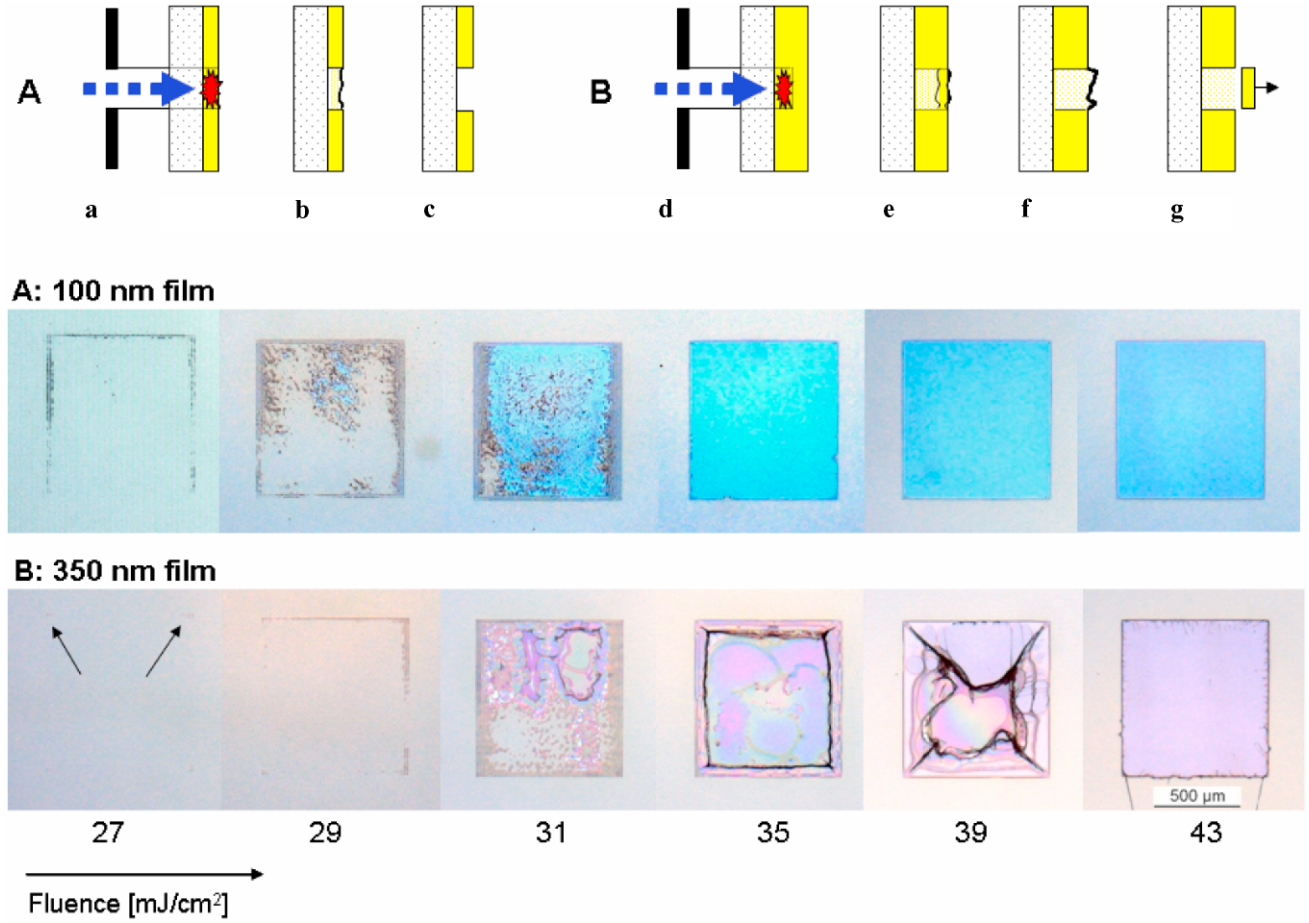

Fig. 6 Perforation behavior and surface morphology of (A) a 100 nm, and (B) a 350 nm thick film of TP-6-Me after single-pulse irradiation from the reversed side (without a receiving substrate), depending on the film thickness and the fluence. In sketches (**a**)–(**g**) schematic cross sections are shown for the laser-induced photodecomposition and forward ejection process within the two films at increasing fluences. The two rows of corresponding microscopy images illustrate the experimental findings at the given fluences closely above the surface perforation threshold (see text for details)

is sufficient to overcome the mechanical resistance and cohesion of the remaining overlying film material. For that reason, films with a thickness above a critical ablation depth might exhibit a different morphological behavior for single-pulse forward ablation than thinner ones. A remaining lid layer of nonablated polymer should stay on top of the in part ablated spot caves (cf. sketches d to f in Fig. 6), affording an insight in the film delamination behavior and morphological changes of the irradiated polymer. In order to check that hypothesis, we investigated a series of our photopolymer films with thicknesses between 25 nm and more than 350 nm. Some typical results of these basic forward ablation experiments are compiled in Fig. 6 for two films of TP-6-Me with a thickness of 100 nm and 350 nm. The microscope pictures show the top surface of the photopolymer films after single-pulse irradiation from the reversed side through the quartz carrier at six increasing laser fluences between 27 mJ/cm^2 and 43 mJ/cm^2. For the 100 nm thick film one can recognize the emerging rectangular spot shape of the mask projection as a fine dark line pattern in the top layer already at a fluence of ~27 mJ/cm^2. This value represents the onset of the beginning surface perforation. At slightly higher fluences between ~29 mJ/cm^2 and ~31 mJ/cm^2, respectively, a progressive but incomplete photodecomposition of the irradiated layer area can be observed, with some degraded areas remaining on the substrate. Interestingly, no particulate fragments or grainy debris were found around the perforated or ablated spots. This can obviously be seen as a hint that the photofragmentation process generates preferentially gaseous and volatile cleavage products which can perforate the top lid layer and permeate through the remaining thin skin. Already at a fluence of ~35 mJ/cm^2 a homogeneous appearance of the area within the ablated spot can be seen which indicates that the polymer has obviously been removed to a large extent, even when the border lines of the crater are yet a bit fringed. Above fluences of ~39 mJ/cm^2 the remaining spots appear uniformly clean

and the morphology of the spot edges is remarkably sharp and straight cut.

Corresponding results of forward-ablation experiments performed with a 350 nm thick film at the same fluences are shown in the second row of images in Fig. 6. The onset of emerging surface perforation appears here at a fluence of ~29 mJ/cm^2, even when the pattern appears weaker and not so sharp drawn as for the 100 nm thick film. At a fluence of ~31 mJ/cm^2 one can observe an irregularly decomposed remaining layer with holes and bubble formation. Obviously, the gaseous pressure-promoted fragmentation products permeate from the underlying spot cavity through the remaining polymer top skin, inducing there a certain mechanical stress loading and partial degradation. Some of our forward-ablation experiments performed at laser fluences around ~35 mJ/cm^2 led to the formation of spot cavities without perforation holes within the remaining top layer of the thin film, corresponding to sketch e in Fig. 6. An intact and transparent ultrathin skin layer stays preserved (keeping the decomposition products trapped inside the ablated cave). This situation is presented in Fig. 6 for the spot created at a fluence of 35 mJ/cm^2 in the 350 nm thick polymer film (row B). Nevertheless, the remaining thin top membrane shows clearly discernible morphological alterations in form of dark lines along the inner spot boundaries. Obviously, the expansion of the gaseous photofragmentation products inflated the ablated cave volume and led to a mechanical stretching of the lid layer, but was not sufficient to perforate it. A similar effect (referred to as "balloon effect") was observed also for the IR laser-induced ablation of an elastic silicone layer coated on top of an energetic nitrocellulose-based DRL [44], and very recently, a corresponding permanent mechanical bulge deformation has been reported for a related LIFT experiment with a 4 μm thick polyimide film as the DRL using a pulsed 355 nm laser [45]. At further increasing fluences the remaining top layer structures were mainly ruptured and showed typically dark colored cross-lines between the diagonal corners of the square spot, resembling spider web structures. The remaining parts of the perforated polymer skin show unambiguous traces of severe mechanical deformation and stretching, probably enhanced by thermal degradation processes. Above fluences from ~43 mJ/cm^2 to about 50 mJ/cm^2 the degraded layer structures were completely delaminated and punched out with clean and sharp-cut borders of the ablation spot. Some of the forward-ejected lid residues could in part be found scattered over the adjacent substrate surface as fibrous debris. The experimental fact that at a laser fluence of about 50 mJ/cm^2 a well-defined spot volume can be completely delaminated and forward-ablated even in a 350 nm thick photopolymer film demonstrates clearly the powerful mechanical effects caused by the laser-triggered pressure-generation which can be utilized for the forward-ejection of overlying materials.

3.3 Fundamental transfer studies

In order to investigate the lift-off and transfer behavior in the presence of a receiver substrate basic transfer experiments were performed with films of TP-6-Me as a monolayered donor model system. In Fig. 7 some results for the DRL test system with a film thickness of 150 nm are summarized. With this film thickness we could observe the transfer and deposition of a thin top flyer of the propelled DRL photopolymer material itself, as outlined in sketches a–c in Fig. 7. The outcome of these single-pulse LIFT experiments is illustrated for six increasing laser fluences on the basis of pairs of microscope images taken from both, the backside ablated spots on the donor substrates (D, the left column) as well as from the corresponding deposited flyer on the receiver surface (R, the right column). The micrographs were taken after separation of the two carrier substrates. Image pairs 1 and 2 present ablation spots after backside irradiation at the onset regime of transfer at laser fluences of 31 mJ/cm^2 and 37 mJ/cm^2, respectively. The starting perforation of the donor top surface can be recognized, and only incomplete and rough structures were deposited on the receiver. As can be seen from spot pair 4, created at a laser fluence of around 66 mJ/cm^2, a well-defined shape of the outlines with sharp rims and a nearby uniform appearance of the surface morphology was obtained for both, the donor spot as well as for the transferred pixel. No further remarkable changes of the spot morphology or quality of the rim structures can be seen from spot pairs 5 and 6 where a laser fluence of 90 mJ/cm^2 and 105 mJ/cm^2, respectively, was applied for the transfer experiments.

The deposited intact polymer pixels showed a remarkable adhesion to the surface of the receiving fused silica substrate keeping the layer from delaminating, even upon subsequent micromechanical manipulation by the profilometer tip during surface morphology analyses. The adhesion behavior depends clearly on the material properties of the transferred layer which influence the adhesive interface interactions between the deposited flyers and the receiving surface. It is an empirical fact that numerous polymers in the rubbery state show an increased stickiness that makes adhesion to surfaces easier than in the glassy state. Thin films of the applied photopolymer TP-6-Me—which has a glass transition temperature T_g of about 50°C—show excellent adhesion to the surface of the used quartz carrier substrates, especially after annealing at 60—70°C (i.e., the drying step after film deposition by spin-coating) [37]. This temperature might be easily exceeded during the ejection process of the flyer, so that the polymer pixels might be transferred in an elastoplastic state and deposited with a high, fluence-dependent impact. First results of our recently published transfer studies with different polymer top layers [41] suggest that the adhesion as well as the integrity of the transferred layers depend also on the applied laser fluence.

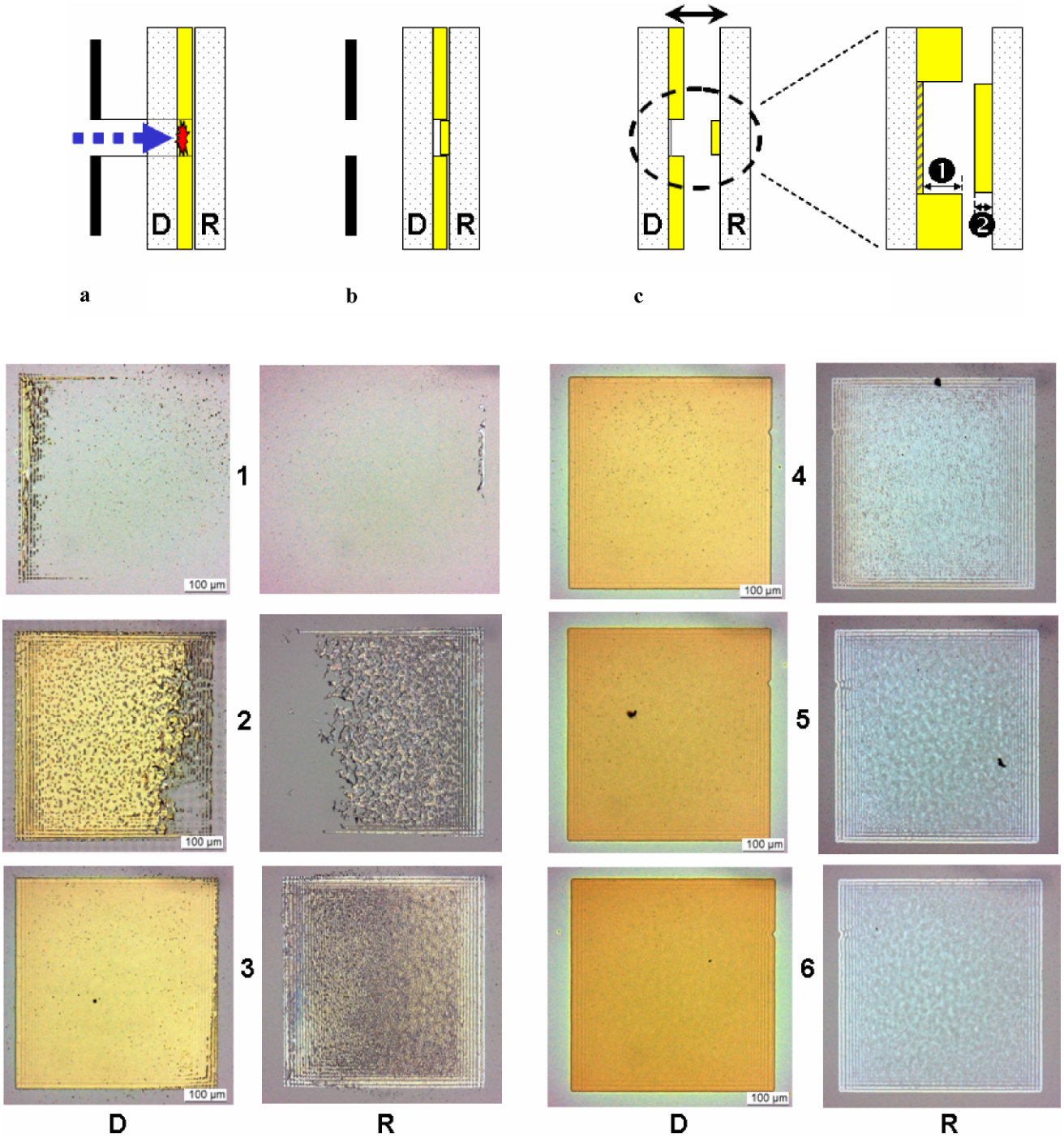

Fig. 7 Forward transfer of a 150 nm thick film of the photopolymer TP-6-Me (coated onto the donor D) towards a receiving substrate R mounted in close contact to the donor. After laser irradiation (**a**) the donor-receiver pair with the transferred flyer pixel (**b**) is separated (**c**). The microscopy images show six corresponding donor-receiver pairs after single-pulse LIFT at increasing laser fluences, and after separation of the substrates: Laser fluences were (1): 31; (2): 37; (3): 47; (4): 66; (5): 90; and (6): 105 mJ/cm^2, respectively. Black spots on the surface stem from dust particles deposited on the samples after separation of the substrates

The deposited pixels on the receiver as well as the corresponding ablated donor spots were analyzed by profilometry. The plot shown in Fig. 8 represents both the determined ablation depths within the donor films D (❶, see also Fig. 7, sketch c) as well as the heights of the deposited polymer pixels (❷) on the receiver R versus the applied fluence. With increasing laser fluences the depth of the forward-ablated donor spots reaches nearly the original film thickness, but

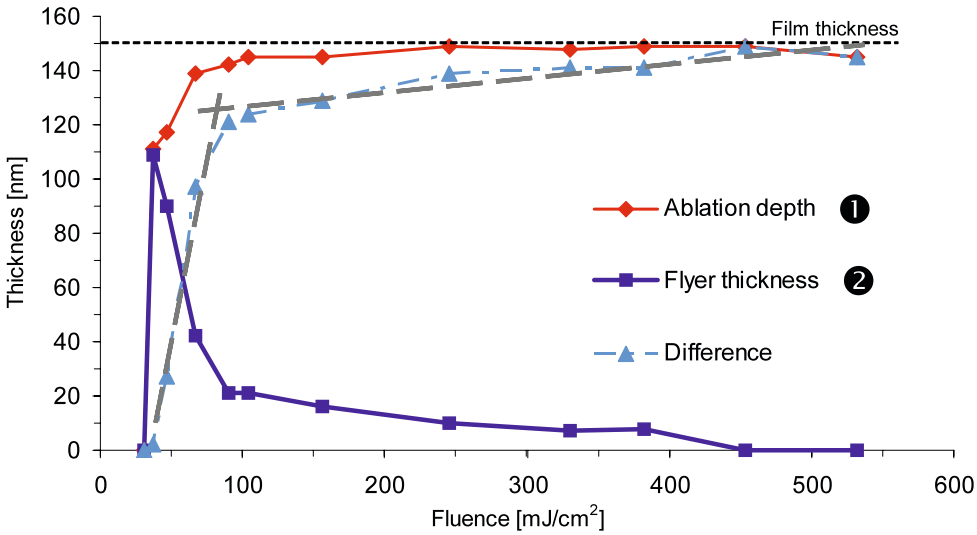

Fig. 8 Correlation between the ablation depth on the donor substrate and the thickness of the transferred flyer pixel for a 150 nm thick film of TP-6-Me. The dashed gray difference curve represents the amount of decomposed photopolymer

we found for some samples a very thin remaining layer on the source substrate. Evidently, not all photopolymer gets completely detached from the irradiated interface area, but the mechanistic reasons for these persistent residues are not yet elucidated. On the other hand, the layer thickness of the transferred polymer pixels exhibits a much stronger dependence from the applied laser fluence and reaches a certain plateau domain of around 20 nm for laser fluences between ~90 and ~150 mJ/cm^2. The thickness for the integrally deposited pixel of image pair 4 was ~45 nm, whereas the corresponding donor spot shows an ablated depth of about 140 nm. Therefore, related to the initial film thickness of ~150 nm, a difference in height of about 90 nm is missing. The corresponding amount of photopolymer has obviously been consumed and decomposed as the sacrificial propellant during the transfer process. The dashed (gray) curve in the graph in Fig. 8 represents these differences and indicates therefore the amount of decomposed polymer. For the simple model transfer system of the photopolymer itself, the difference curve shows clearly two well-distinguishable process domains which seem to have a transition in the region of about 80 mJ/cm^2 for the 150 nm thick photopolymer film. Above this value the structure morphology of transferred pixels showed conserved integrity. A decrease of the transferred film thickness with increasing laser fluences can be explained in part with the increasing UV light penetration of the donor film at higher fluences due to an enhanced photodecomposition process within the irradiated film. Therefore, the processing window for the transfer of intact 20 nm thick polymer pixels was found to be approximately in the range of 100 mJ/cm^2.

4 Summary and conclusions

Basic process parameters for the conventional laser ablation of films of photopolymer TP-6-Me were determined and put in relation with data derived from forward ablation experiments. Resulting effects of the irradiation from the backside on the ablative photodecomposition behavior and forward ejection of the polymer were studied. The processing window for a controllable thin-layer transfer of a 150 nm thick DRL model system was found to be in the range of laser fluences between ~80–100 mJ/cm^2 and about 350 mJ/cm^2 resulting in the deposition of about 10–20 nm thick intact polymer pixels. In order to derive optimum process conditions for photopolymer-based DRL systems for LIFT applications, more detailed studies of the various influences of material properties [41] and photophysical effects on the resulting mechanisms of the transfer processes [46] and the extent of possibly occurring thermally or photochemically induced degradation effects are currently under extensive investigation.

Acknowledgements Financial Support from Swiss National Science Foundation is gratefully acknowledged.

References

1. C.B. Arnold, P. Serra, A. Piqué, MRS Bull. **32**, 23–31 (2007)
2. V.S. Ban, D.A. Kramer, J. Mater. Sci. **5**(11), 978–982 (1970)
3. S. Hansen, T. Robitaille, Appl. Phys. Lett. **50**(6), 359–361 (1987)
4. N. Matsumoto, H. Shima, T. Fujii, F. Kannari, Appl. Phys. Lett. **71**(17), 2469–2471 (1997)
5. X. Yang, Y. Tang, M. Yu, Q. Qin, Thin Solid Films **358**, 187–190 (2000)
6. G. Blanchet, Macromolecules **28**, 4603–4607 (1995)
7. D. Chrisey, A. Piqué, R. McGill, J. Horwitz, B. Ringeisen, D. Bubb, P. Wu, Chem. Rev. **103**, 553–576 (2003)
8. D. Chrisey, A. Piqué, J. Fitz-Gerald, R. Auyeung, R. McGill, H. Wu, M. Duignan, Appl. Surf. Sci. **154–155**, 593–600 (2000)
9. K. Kyrkis, A. Andreadaki, D. Papazoglou, I. Zergioti, in *Recent Advances in Laser Processing of Materials*, ed. by J. Perrière, E. Millon, E. Fogarassy (Elsevier, Amsterdam, 2006), pp. 213–241, and references therein

10. A. Klini, A. Mourka, V. Dinca, C. Fotakis, F. Claeyssens, Appl. Phys. A **87**, 17–22 (2007)
11. C. Germain, L. Charron, L. Lilge, Y.Y. Tsui, Appl. Surf. Sci. **253**, 8328–8333 (2007)
12. B.R. Ringeisen, C.M. Othon, J.A. Barron, D. Young, B.J. Spargo, Biotechnol. J. **1**, 930–948 (2006)
13. A. Karaiskou, I. Zergioti, C. Fotakis, M. Kapsetaki, D. Kafetzopoulos, Appl. Surf. Sci. **245–249**, 245–249 (2003)
14. I. Zergioti, A. Karaiskou, D.G. Papazoglou, C. Fotakis, M. Kapsetaki, D. Kafetzopoulos, Appl. Surf. Sci. **247**, 584–589 (2005)
15. Y. Tsuboi, Y. Furuhata, N. Kitamura, Appl. Surf. Sci. **253**, 8422–8427 (2007)
16. W.A. Tolbert, I.-Y. Sandy Lee, X. Wen, D.D. Dlott, M.M. Doxtader, E.W. Ellis, J. Imaging Sci. Technol. **37**, 485–489 (1993)
17. G.R. Pinto, J. Imaging Sci. Technol. **38**, 565–570 (1994)
18. P. Serra, M. Colina, J.M. Fernández-Pradas, L. Sevilla, J.L. Morenza, Appl. Phys. Lett. **85**, 1639–1641 (2004)
19. P. Serra, J.M. Fernández-Pradas, F.X. Berthet, M. Colina, J. Elvira, J.L. Morenza, Appl. Phys. A **79**, 949–952 (2004)
20. J.M. Fernandez-Pradas, M. Colina, P. Serra, J. Dominguez, J.L. Morenza, Thin Solid Films **453–454**, 27–30 (2004)
21. V. Dinca, E. Kasotakis, J. Catherine, A. Mourka, A. Mitraki, A. Popescu, M. Dinescu, M. Farsari, C. Fotakis, Appl. Surf. Sci. **254**, 1160–1163 (2007)
22. B. Hopp, T. Smausz, N. Kresz, N. Barna, Z. Bor, L. Kolozsvari, D.B. Chrisey, A. Szabo, A. Nogradi, Tissue Eng. **11**, 1817–1823 (2005)
23. B. Hopp, T. Smausz, Z. Antal, N. Kresz, Z. Bor, D. Chrisey, J. Appl. Phys. **96**, 3478–3481 (2004)
24. B. Hopp, T. Smausz, N. Barna, C. Vass, Z. Antal, L. Kredics, J. Phys. D: Appl. Phys. **38**, 833–837 (2005)
25. T. Smausz, B. Hopp, G. Kecskemeti, Z. Bor, Appl. Surf. Sci. **252**, 4738–4742 (2006)
26. J.A. Barron, P. Wu, H.D. Ladouceur, B.R. Ringeisen, Biomed. Microdevices **6**, 139–147 (2004)
27. M. Irie, T. Kitamura, J. Imaging Sci. Technol. **37**, 231–234 (1993)
28. M. Irie, Jpn. J. Appl. Phys. **42**, 1633–1636 (2003)
29. M. Kinoshita, K. Hoshino, T. Kitamura, J. Imaging Sci. Technol. **44**, 105–110 (2000)
30. G.B. Blanchet, Y.-L. Loo, J.A. Rogers, F. Gao, C.R. Fincher, Appl. Phys. Lett. **82**, 463–465 (2003)
31. M.C. Suh, B.D. Chin, M.-H. Kim, T.M. Kang, S.T. Lee, Adv. Mater. **15**, 1254–1258 (2003)
32. J.Y. Lee, S.T. Lee, Adv. Mater. **16**, 51–54 (2004)
33. M.B. Wolk, J. Baetzold, E. Bellmann, T.R. Hoffend, S. Lamansky, Y. Li, R.R. Roberts, V. Savvateev, J.S. Staral, W.A. Tolbert, Proc. SPIE **5519**, 12–23 (2004)
34. S. Lamansky, T.R. Hoffend, H. Le, V. Jones, M.B. Wolk, W.A. Tolbert, Proc. SPIE **5937**, 593702 (2005)
35. T. Lippert, Adv. Polym. Sci. **168**, 51–246 (2004), and references therein
36. T. Lippert, T. Dickinson, Chem. Rev. **103**, 453–485 (2003)
37. M. Nagel, R. Hany, T. Lippert, M. Molberg, F.A. Nüesch, D. Rentsch, Macromol. Chem. Phys. **208**, 277–286 (2007)
38. A. Doraiswamy, R.J. Narayan, T. Lippert, L. Urech, A. Wokaun, M. Nagel, B. Hopp, M. Dinescu, R. Modi, R.C.Y. Auyeung, D.B. Chrisey, Appl. Surf. Sci. **252**, 4743–4747 (2006)
39. J. Xu, J. Liu, D. Cui, M. Gerhold, A.Y. Wang, M. Nagel, T.K. Lippert, Nanotechnology **18**, 025403 (2007)
40. R. Fardel, M. Nagel, F. Nüesch, T. Lippert, A. Wokaun, Appl. Phys. Lett. **91**, 061103 (2007)
41. R. Fardel, M. Nagel, F. Nüesch, T. Lippert, A. Wokaun, Appl. Surf. Sci. **254**, 1322–1326 (2007)
42. R. Fardel, P. Feurer, T. Lippert, M. Nagel, F.A. Nüesch, A. Wokaun, Appl. Surf. Sci. **254**, 1332–1337 (2007)
43. H. Furutani, H. Fukumura, H. Masuhara, T. Lippert, A. Yabe, J. Phys. Chem. A **101**, 5742–5747 (1997)
44. D.D. Dlott, Appl. Surf. Sci. **197–198**, 3–10 (2002)
45. N.T. Kattamis, P.E. Purnick, R. Weiss, C.B. Arnold, Appl. Phys. Lett. **91**, 171120 (2007)
46. R. Fardel, M. Nagel, T. Lippert, F. Nüesch, A. Wokaun, B.S. Luk'yanchuk, Appl. Phys. A **90**, 661–667 (2008)